PARAMETER ESTIMATION OF A VECTOR HYSTERESIS MODEL USING GENETIC ALGORITHMS

Data de submissão: 26/12/2024 *Data de aceite: 02/01/2025*

Lesly Daiana Barbosa Sobrado
Universidade Federal do Rio de Janeiro, Instituto de Matemática Rio de Janeiro – Rio de Janeiro
http://lattes.cnpq.br/5520816294622415

Filomena Barbosa Rodrigues Mendes
Universidade Tecnológica Federal do Paraná, Departamento Acadêmico de Elétrica
Pato Branco - Paraná
http://lattes.cnpq.br/1945890297316691

Jean Vianei Leite
Universidade Federal de Santa Catarina, Grupo de Concepção e Análise de Dispositivos Eletromagnéticos
Florianópolis – Santa Catarina
http://lattes.cnpq.br/8595245291065003

Nelson Jhoe Batistela
Universidade Federal de Santa Catarina, Grupo de Concepção e Análise de Dispositivos Eletromagnéticos
Florianópolis – Santa Catarina
http://lattes.cnpq.br/5387328100140459

ABSTRACT: The laboratory for designing and analyzing electromagnetic devices (GRUCAD) received samples of non-oriented grain silicon steel. Two measurements of the magnetic field strength versus magnetic flux density curves were performed. This chapter presents a novel method for extracting the ten bidimensional magnetic hysteresis parameters of the Jiles-Atherton vector model to model the experimental curves. The procedure is based on the genetic algorithms method and ensures a strong agreement between the calculated hysteresis and the experimental curves. This provides reliable validation for the ten computed parameters. Additionally, the paper demonstrates a practical application of these parameters. With the ten parameters, it is possible to obtain two anhysteretic curves. The ascending data in the first quadrant represents the initial magnetization curve of the material. These initial magnetization curves are then used in the Ansys Electromagnetics Suite software to define the nonlinear anisotropic core of an alternating current inductor. Subsequently, a two-dimensional finite element analysis is performed. The analysis improves the design and computation of inductors extensively utilized in electrical engineering. This study contributes to understanding and optimizing inductors, promoting significant advancements in electrical engineering.

KEYWORDS: Finite element method.

Genetic algorithms method. Magnetic anisotropy. Magnetic hysteresis.

BUSCA DE PARÂMETROS DE UM MODELO DE HISTERESE VETORIAL UTILIZANDO ALGORITMOS GENÉTICOS

RESUMO: O Grugo de Concepção e Análise de Dispositivos Eletromagnéticos (GRUCAD) recebeu amostras de aço silício de grão não orientado. Foram realizadas duas medições das curvas de campo magnético versus Indução magnética. Este trabalho apresenta um método inovador para extrair os dez parâmetros bidimensionais de histerese magnética do modelo vetorial de Jiles- Atherton, visando modelar as curvas experimentais. O procedimento é baseado no método de algoritmos genéticos e garante uma forte concordância entre as curvas calculadas de histerese e as curvas experimentais. Isso proporciona uma validação confiável para os dez parâmetros calculados. Além disso, o artigo demonstra uma aplicação prática desses parâmetros. Com os dez parâmetros, é possível obter duas curvas anhistéricas. Os dados ascendentes no primeiro quadrante representam a curva de magnetização inicial do material. Essas curvas de magnetização inicial são então utilizadas no software Ansys Electromagnetics Suite para definir o núcleo não linear anisotrópico de um indutor de corrente alternada. Subsequentemente, uma análise de elementos finitos bidimensional é realizada. Essa análise aprimora o projeto e o cálculo de indutores amplamente utilizados na engenharia elétrica. Este trabalho contribui para o entendimento e a otimização de indutores, promovendo avanços significativos na engenharia elétrica.
PALAVRAS-CHAVE: Método de elementos finitos. Método de algoritmos genéticos. Anisotropia magnética. Histerese magnética.

1 I INTRODUCTION

Over time, several studies have been done [1] - [25] to improve the design of electromagnetic devices. These studies focus on mathematically modeling the ferromagnetic hysteresis phenomenon. The efforts include obtaining model parameters using genetic algorithms, analyzing complicated structures using the finite element method, and predicting the behavior of materials in electrical machines, all before the prototype construction.

The hysteresis model developed by David Jiles and David Atherton [1] is an important tool for analyzing the magnetic behavior of ferromagnetic materials, especially in magnetization and demagnetization cycles. This model can represent the nonlinear magnetic response of such materials in electromagnetic systems. The model is based on the theory of magnetic hysteresis, which studies how ferromagnetic materials resist changes in their magnetic field strength through nonlinear differential equations. These equations describe the relationship between the applied magnetic field strength, the resulting magnetic flux density, and other parameters. The Jiles-Atherton model is valuable in computational simulations of complicated magnetic systems, such as transformers, inductors, contactors, motors, and electrical generators. It accurately captures nonlinear behavior and magnetic hysteresis, enabling refined performance analysis of systems under different operational

conditions. The model was first published in 1986, based on thermodynamic energy principles and considering magnetic interactions. In the 1990s, extensions were made to cover different types of materials, and in the early 2000s, adaptations were made to handle high frequencies. Internationally adopted, the model simulates hysteresis curves, providing accurate predictions of magnetic behavior in applications within electrical engineering, electronics, and materials science. Research continues to improve the model's accuracy, including thermal considerations. In summary, the Jiles-Atherton hysteresis model is an indispensable tool for understanding and simulating the magnetic behavior of ferromagnetic materials, which is important for the efficient design of electromagnetic devices in electrical and electronic engineering.

The theory of genetic algorithms originated in the 1940s and experienced significant advances in the 1950s, based on the principles of evolutionary theory. In 1962, the first models were conceived, marking the beginning of this innovative approach. The method became popular in 1975 and solidified with applications in various fields during the 1980s. In 1989, we witnessed the emergence of the first commercial software dedicated to genetic algorithms. In the 1990s, these algorithms were incorporated into college courses and motivated the development of open-source libraries. The turn of the millennium marked the formalization of conferences focused on genetic algorithms.

Genetic algorithms [5] [6], as a computational method, draw inspiration from natural selection. This approach finds application in solving complicated optimization and search problems in various fields, including engineering, computer science, finance, and computational biology. This methodology is based on natural selection, crossover, mutation, and heredity. Solution candidates are represented by data structures called chromosomes. Each chromosome has genes representing the solution's variables, and the process starts with creating an initial population of randomly generated chromosomes. During the step of evaluating fitness, each chromosome is checked to see if it can solve the problem. A fitness function evaluates how well a solution represents the desired result by assigning a value. Natural selection favors the most competent chromosomes for reproduction. Crossover, in which selected pairs are combined, occurs at specific points on the chromosomes, promoting the mixing of genetic information. Mutation, with the introduction of random genetic alterations, contributes to genetic diversity in the population. Chromosomes in the new generation are formed from the offspring created through crossover and mutation. This new population is once again subjected to a fitness evaluation. The algorithm is iterated over several generations until a stopping criterion is met, which may be a maximum number of generations, convergence to an acceptable solution, or other criteria.

The finite element method was first used in the 1940s to analyze aircraft structures. Over the years, its application expanded: in the 1950s, this method was adopted in civil and mechanical engineering. The term finite elements and its applications in engineering began in the 1960s. In the 1970s, commercial software for the finite element method became

widely adopted due to technological advancements. In the 1990s, this method evolved to address nonlinear and multiphysics problems, expanding its analytical capabilities. In 2010, the finite element method was used in optimization problems. The 2020s witnessed the application of the technique in innovative domains such as machine learning. In biomedical engineering, the finite element method is important for analyzing prosthetics. It is commonly used to evaluate wind turbines and solar panels, helping to advance renewable energy. The trajectory of the finite element method illustrates its continuous evolution, from its origins in aviation to its current applications in various fields, establishing itself as an essential tool in modern engineering.

The finite element method [10]-[20] is a widely used numerical technique for analyzing the behavior of complicated devices and solving engineering problems. When using finite elements to model a device, start by identifying the physical problem that can be mathematically modeled. The geometry of the device is divided into small regions called finite elements. Physical and material properties are assigned to the elements to represent the actual behavior of the device under analysis. Mathematical equations that describe the behavior of each element are formulated. The local equations of each element are combined to form a global system of equations that describes the behavior of the entire device. These equations consider the boundary conditions of the problem. The resulting system of equations is solved to obtain a numerical solution that represents the unknown variables. This solution is analyzed by visualizing graphs and interpreting data to make engineering decisions. The finite element method is versatile and is applied in various fields, including electromagnetism. It allows for the efficient and accurate simulation of the behavior of complicated devices, making it a valuable tool in the analysis and optimization of device designs.

2 | GENETIC ALGORITHMS

A method based on genetic algorithms was adopted for the identification of the 10 parameters of the two-dimensional hysteresis model of Jiles-Atherton, with 5 longitudinal x and 5 transverse y parameters: $5P_X = [m_{sx}\ \alpha_x\ a_x\ k_x\ c_x]$ and $5P_Y = [m_{sy}\ \alpha_y\ a_y\ k_y\ c_y]$. The main steps of the method are as follows: create the initial generation, evaluate it, form the subsequent generation, and analyze it again.

For the first-generation

1) Define the range of variation for each parameter: $\min \leq m_{sx} \leq \max$, $\min \leq \alpha_x \leq \max$, …, $\min \leq c_x \leq \max$, $\min \leq m_{sy} \leq \max$, $\min \leq \alpha_y \leq \max$, …, $\min \leq c_y \leq \max$.

2) Generate 100 random values within the established range for each parameter: $[m_{sx}(1)\ \alpha_x(1)\ a_x(1)\ k_x(1)\ c_x(1)]$, …, $[m_{sx}(100)\ \alpha_x(100)\ a_x(100)\ k_x(100)\ c_x(100)]$ and $[m_{sy}(1)\ \alpha_y(1)\ a_y(1)\ k_y(1)\ c_y(1)]$, …, $[m_{sy}(100)\ \alpha_y(100)\ a_y(100)\ k_y(100)\ c_y(100)]$.

3) Record the experimental magnetic flux density values (B_x and B_y) along the curves

H_xB_x and H_yB_y.

4) Calculate the magnetic field strength H_x using the inverse Jiles-Atherton model proposed by GRUCAD for the first individual of the population*x* [$m_{sx}(1)$ $\alpha_x(1)$ $a_x(1)$ $k_x(1)$ $c_x(1)$]. Similarly, calculate the magnetic field strength H_y for the first individual of the population*y* [$m_{sy}(1)$ $\alpha_y(1)$ $a_y(1)$ $k_y(1)$ $c_y(1)$].

5) Compare the calculated magnetic field strength with the experimental magnetic field strength along the *HB* curve, allowing for the determination of the sum of the relative error.

6) Repeat steps 4 and 5 for the other individuals in the population.

7) Record the data obtained.

8) Organize data in ascending order of error and evaluate the initial population*x*, assigning a maximum fitness of 2 to the individual with the smallest error and a minimum fitness of 0 to the individual with the largest error.

9) Repeat step 8 organizing and evaluating the initial population*y*.

10) Record the fitness values.

For the next generation

1. Randomly select two individuals from the initial population*x*, with the fittest designated as *father* $1_x = [m_{sx(i)}\ \alpha_{x(i)}\ a_{x(i)}\ k_{x(i)}\ c_{x(i)}]$. Establish $father_{2x} = [m_{sx(t)}\ \alpha_{x(t)}\ a_{x(t)}\ k_{x(t)}\ c_{x(t)}]$ through a similar process.

2. Repeat step 1 for the population*y*, identifying $father1_y = [m_{sy(d)}\ \alpha_{y(d)}\ a_{y(d)}\ k_{y(d)}\ c_{y(d)}]$ and $father2_y = [m_{sy(l)}\ \alpha_{y(l)}\ a_{y(l)}\ k_{y(l)}\ c_{y(l)}]$.

3. Apply the BLX-alpha crossover operation between $father1_x = [m_{sx(i)}\ \alpha_{x(i)}\ a_{x(i)}\ k_{x(i)}\ c_{x(i)}]$ and $father_{2x} = [m_{sx(t)}\ \alpha_{x(t)}\ a_{x(t)}\ k_{x(t)}\ c_{x(t)}]$ to generate a longitudinal child $ch_{1x} = [m_{sx}\ \alpha_x\ a_x\ k_x\ c_x]$.

4. Repeat step 3 using $father_{1y} = [m_{sy(d)}\ \alpha_{y(d)}\ a_{y(d)}\ k_{y(d)}\ c_{y(d)}]$ and $father_{2y} = [m_{sy(l)}\ \alpha_{y(l)}\ a_{y(l)}\ k_{y(l)}\ c_{y(l)}]$ to generate a transverse child $ch_{1y} = [m_{sy}\ \alpha_y\ a_y\ k_y\ c_y]$.

5. Randomly select between $father_{1x} = [m_{sx(i)}\ \alpha_{x(i)}\ a_{x(i)}\ k_{x(i)}\ c_{x(i)}]$ or $father_{2x} = [m_{sx(t)}\ \alpha_{x(t)}\ a_{x(t)}\ k_{x(t)}\ c_{x(t)}]$ to undergo mutation: $father_{2x} = [m_{sx(t)}\ \alpha_{x(t)}\ a_{x(t)}\ k_{x(t)}\ c_{x(t)}]$.

6. Randomly select a parameter from the chosen father to undergo mutation*:* $father_{2x} = [m_{sx(t)}\ \alpha_{x(t)}\ a_{x(t)}\ k_{x(t)}\ c_{x(t)}]$.

7. Randomly select between the maximum or minimum value of the parameter and replace that parameter to generate the second longitudinal child with mutation: $ch_{2x} = [m_{sx(t)}\ \alpha_{x(t)}\ \max\ k_{x(t)}\ c_{x(t)}]$.

8. Randomly select between $father_{1y} = [m_{sy(d)}\ \alpha_{y(d)}\ a_{y(d)}\ k_{y(d)}\ c_{y(d)})]$ or $father_{2y} = [m_{sy(l)}\ \alpha_{y(l)}\ a_{y(l)}\ k_{y(l)}\ c_{y(l)}]$ to undergo mutation: $father_{1y} = [m_{sy(d)}\ \alpha_{y(d)}\ a_{y(d)}\ k_{y(d)}\ c_{y(d)}]$.

9. Randomly select a parameter from the chosen father to undergo mutation: $father_{1y} = [m_{sy(d)}\ \alpha_{y(d)}\ a_{y(d)}\ k_{y(d)}\ c_{y(d)}]$.

10. Randomly select between the maximum or minimum value of the parameter and replace that parameter to generate the second transverse child with mutation: ch_{2y} = [min $\alpha_{y(d)}$ $a_{y(d)}$ $k_{y(d)}$ $c_{y(d)}$].

11. The two generated children, ch_{1x} = [m_{sx} α_x a_x k_x c_x] and ch_{2x} = [$m_{sx(t)}$ $\alpha_{x(t)}$ max $k_{x(t)}$ $c_{x(t)}$], replace the two least-fit individuals of the initial population*x*.

12. The two generated children, ch_{1y} = [m_{sy} α_y a_y k_y c_y] and ch_{2y} = [min $\alpha_{y(d)}$ $a_{y(d)}$ $k_{y(d)}$ $c_{y(d)}$], replace the two least-fit individuals of the initial population*y*.

13. For the most recent sample of individuals from Table 1 and Table 2, resume the procedure from step 3 of the first generation section.

Individual	**Parameters: 5***Px*					**Error**	**Fitness**
1	$m_{sx(1)}$	$\alpha_{x(1)}$	$a_{x(1)}$	$k_{x(1)}$	$c_{x(1)}$	$error_{x(1)}$	2
2	$m_{sx(2)}$	$\alpha_{x(2)}$	$a_{x(2)}$	$k_{x(2)}$	$c_{x(2)}$	$error_{x(2)}$	1.98
.	.	.	.	.	.	.	.
.	.	.	.	.	.	.	.
.	.	.	.	.	.	.	.
i	$m_{sx(i)}$	$\alpha_{x(i)}$	$a_{x(i)}$	$k_{x(i)}$	$c_{x(i)}$	$error_{x(i)}$	2(100- *i*)/99
.	.	.	.	.	.	.	.
t	$m_{sx(t)}$	$\alpha_{x(t)}$	$a_{x(t)}$	$k_{x(t)}$	$c_{x(t)}$	$error_{x(t)}$	2(100- *t*)/99
.	.	.	.	.	.	.	.
.	.	.	.	.	.	.	.
.	.	.	.	.	.	.	.
99	m_{sx}	α_x	a_x	k_x	c_x		
100	$m_{sx(t)}$	$\alpha_{x(t)}$	max	$k_{x(t)}$	$c_{x(t)}$		

TABLE 1. Subsequent Longitudinal Population

Individual	**Parameters: 5***Py*					**Error**	**Fitness**
1	$m_{sy(1)}$	$\alpha_{y(1)}$	$a_{y(1)}$	$k_{y(1)}$	$c_{y(1)}$	$error_{y(1)}$	2
2	$m_{sy(2)}$	$\alpha_{y(2)}$	$a_{y(2)}$	$k_{y(2)}$	$c_{y(2)}$	$error_{y(2)}$	1.98
.	.	.	.	.	.	.	.
.	.	.	.	.	.	.	.
.	.	.	.	.	.	.	.
d	$m_{sy(d)}$	$\alpha_{y(d)}$	$a_{y(d)}$	$k_{y(d)}$	$c_{y(d)}$	$error_{y(d)}$	2(100-*d*)/99
.	.	.	.	.	.	.	.
l	$m_{sy(l)}$	$\alpha_{y(l)}$)	$a_{y(l)}$	$k_{y(l)}$	$c_{y(l)}$	$error_{y(l)}$	2(100- *l*)/99
.	.	.	.	.	.	.	.
.	.	.	.	.	.	.	.
.	.	.	.	.	.	.	.
99	m_{sy}	α_y	a_y	k_y	c_y		
100	min	$\alpha_{y(d)}$	$a_{y(d)}$	$k_{y(d)}$	$c_{y(d)}$		

TABLE 2. Subsequent Transverse Population

3 | ACQUIRED PARAMETERS

A Rotational Single Sheet Tester, RSST, was used for the experimental data obtaining. The *HB* curves on the lamination and transversal directions were obtained for an anisotropic silicon steel sample. The experimental device was built with a magnetic yoke, frequency inverters, feedback controllers, magnetic flux density and magnetic field strength sensors, signal amplifiers, signal filters, and boards for generating signals and data acquisition. The yoke of the RSST was made of the overlapping of silicon steel sheets. The excitation coils along the *x* and *y* directions are fed by two independent frequency inverters with pulse width modulation, PWM. Each PWM voltage inverter was driven by an independent closed control loop that imposed the desired magnetic flux density waveform in the sample.

In the GRUCAD laboratory, magnetic field strength values and magnetic flux density measurements were carried out to obtain H_xB_x and H_yB_y curves for five samples of non-oriented grain silicon steel. The genetic algorithm method was employed to calculate the 10 parameters of the Jiles-Atherton vector hysteresis model for these samples. Table 3 presents the 10 calculated parameters for each silicon steel sample, while in Fig. 1 to 5, the agreement between the calculated and experimental *HB* curves for both longitudinal and transverse cases can be observed.

Parameters	Cases				
	1	2	3	4	5
m_{sx}	1.88e+6	1.85e+6	2.28e+6	2.68e+6	1.51e+6
α_x	1.35e-4	1.12e-4	9.70e-5	1.80e-4	1.66e-4
a_x	9.15e+1	9.59e+1	1.74e+2	1.73e+2	9.76e+1
k_x	4.53e+1	5.54e+1	7.30e+1	4.36e+1	6.80e+1
c_x	4.74e-1	1.52e-1	1.70e-1	4.76e-1	1.99e-1
m_{sy}	3.02e+6	2.87e+6	2.11e+6	2.09e+6	1.94e+6
α_y	1.43e-4	1.03e-4	1.36e-5	1.85e-4	2.04e-4
a_y	2.07e+2	1.18e+2	3.37e+1	1.61e+2	2.94e+2
k_y	5.24e+1	2.72e+1	9.43e+1	5.14e+1	6.21e+1
c_y	9.12e-2	2.47e-1	3.71e-1	1.60e-1	1.57e-1

TABLE 3. Acquired Parameters

In Fig. 1 to 5, the ten calculated parameters accurately describe the material's experimental behavior, showing a clear agreement between the simulated and measured *HB* curves. This indicates that the computed parameters perform well in predicting the magnetic behavior of the silicon steel sample, making them useful for application in the construction of electromagnetic devices.

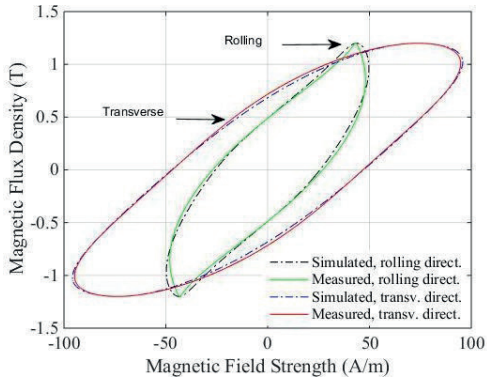

FIGURE 1. Magnetic flux density as a function of applied magnetic field strength. Case 1.

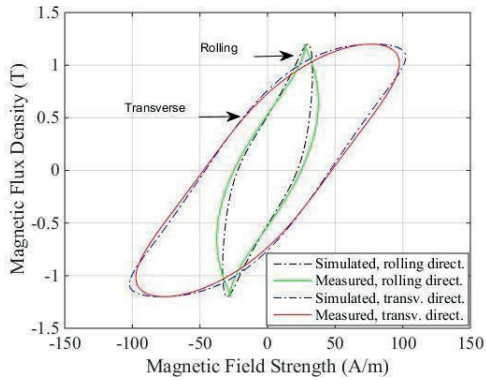

FIGURE 2. Magnetic flux density as a function of applied magnetic field strength. Case 2.

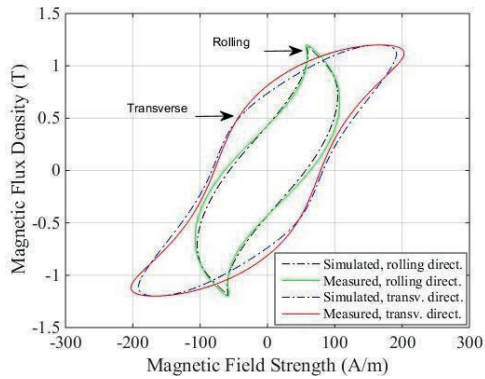

FIGURE 3. Magnetic flux density as a function of applied magnetic field strength. Case 3.

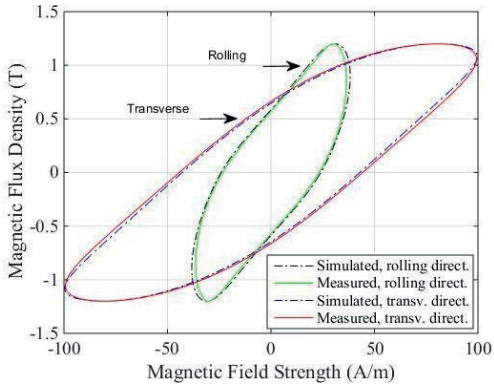

FIGURE 4. Magnetic flux density as a function of applied magnetic field strength. Case 4.

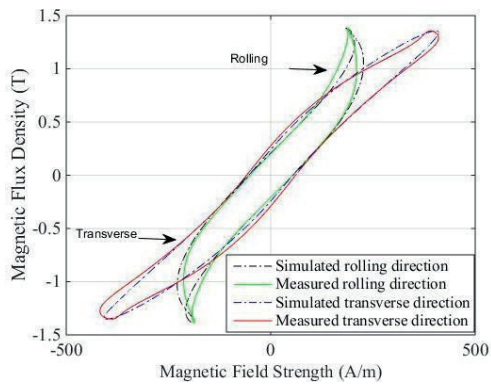

FIGURE 5. Magnetic flux density as a function of applied magnetic field strength. Case 5.

4 | APPLICATION OF PARAMETERS FOR AN INDUCTOR WITH AN ANISOTROPIC CORE

The parameters derived in the fourth case were used in modeling the anisteretic curve according to procedure (1) developed by GRUCAD, maintaining the general nature of the process.

$$
\begin{aligned}
&B_x(i+1) = B_m \sin\left(2\pi f t(i)\right)\\
&\frac{dM_{an}}{dH_e} = \frac{M_{sx}}{a_x}\left[1-\left(\coth\left(\frac{H_e(i)}{a_x}\right)\right)^2+\left(\frac{a_x}{H_e(i)}\right)^2\right]\\
&H_x(i+1) = \Delta M\left[\frac{1}{\frac{dM_{an}}{dH_e}}-\alpha_x\right]+H_x(i) \qquad (1)\\
&M(i+1) = \frac{B_x(i+1)}{\mu_0}-H_x(i+1)\\
&H_e(i+1) = H_x(i+1)+\alpha_x M(i+1)\\
&\Delta M = M(i+1)-M(i)
\end{aligned}
$$

In which: i is the current iteration, B_m is the magnetic flux density in T, f is the frequency in Hz, t is the time in s, M_{an} is the anisteretic magnetization, H_e is the effective magnetic field, M the magnetization and $\mu 0$ is the magnetic permeability of the vacuum.

When following procedure (1), only the ascending points (H_x, B_x) in the first quadrant of the longitudinal anhysteretic curve are important for the initial magnetization curve. Likewise, procedure (1) defines the ascending points (H_y, B_y) in the first quadrant of the transverse anhysteretic curve.

The two-dimensional Cartesian transient magnetic analysis of the inductor was conducted using the software Ansys® Electromagnetics Suite, Release 2022 R2 acquired by UTFPR, following the essential steps:

1. Draw the Inductor: draw the two-dimensional sketch of the inductor, consisting of the coil, E-I core, and the simulation region. The E lamination measures 10.49 cm in length, 6.99 cm in height, and has a central column that is 3.49 cm long. The I lamination has a height of 1.75 cm.

2. Define the Materials of the Inductor: copper was chosen for the coil, and non-oriented grain silicon steel was incorporated into the library and specified for the core. The relevant parameters for this material are presented in Table 3, case 4, showing anisotropic relative magnetic permeability. This nonlinear anisotropy is characterized by first-quadrant ascending anhysteretic *HB* curves, H_xB_x and H_yB_y, as outlined in (1). The vacuum was selected for the simulation region.

3. Assign excitation: a voltage of $127\sin(2\pi 60t)$ Volts was assigned to the coil with 314 turns.

4. Consider eddy effects, boundary, and depth: the evaluation of eddy effects is not conducted due to multiple wires in the coil. The boundary condition for the four edges of the simulation region was vector potential $A = 0$ Wb/m. The depth of the inductor was 34.93 mm.

5. Configure the mesh: define the maximum number of mesh elements for the coil, core, and simulation region of the inductor.

6. Run simulation: establish the analysis setup and initiate the simulation. The transient magnetic simulation of the inductor was briefly conducted, indicating a well-conditioned problem. In Fig. 6, the magnetic flux density reaches 0.10 T in the simulation region and coils. At the eight corners of the core windows, the magnetic flux density is approximately 0.99 T. In the core, magnetic flux density values predominantly range between 0.49 and 0.59 T. Another significant result, presented in Fig. 7, illustrates the nonsinusoidal behavior of the flux linkage, current, and induced voltage over time. The maximum induced voltage reaches 125.93 V, the maximum current is approximately 0.07 A, and the maximum flux linkage is 0.67 Wb. The expected average inductance for the inductor is 0.38 H.

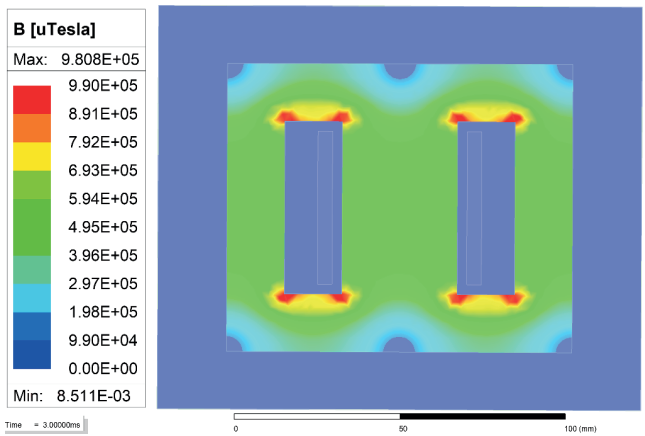

FIGURE 6. Density plot of magnetic flux density in the inductor: non-linear anisotropic core. The values of magnetic flux density are in microtesla.

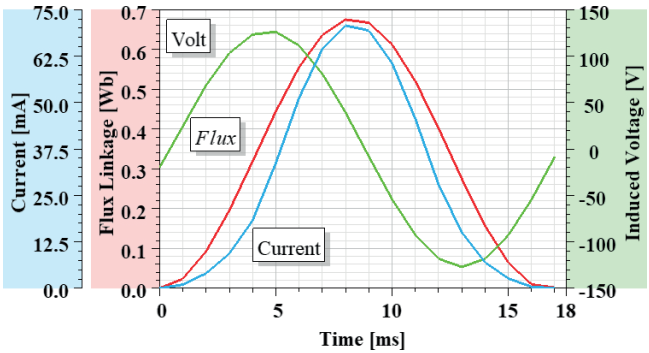

FIGURE 7. Flux linkage, current, and induced voltage in the inductor: non-linear anisotropic core.

5 | APPLICATION OF LONGITUDINAL PARAMETERS FOR AN INDUCTOR WITH A NON-LINEAR CORE

In this analysis, the procedures outlined in section 4 were rigorously followed. The only distinction is that, for the core, a nonlinear relative magnetic permeability was defined, represented by an anisteretic *HB* curve, located in the first quadrant with an ascending path H_xB_x.

Fig. 8, shows that the magnetic flux density reaches 0.09 T in the simulation region and the coils, while at the eight corners of the core windows, the magnetic flux density reaches 0.87 T. The core's magnetic flux density predominantly ranges between 0.61 and 0.70 T. Another important result is the non-sinusoidal behavior of the flux linkage, current, and induced voltage over time. The induced voltage reaches its maximum value of 125.97 V, the maximum current is 0.03 A, and the flux linkage peaks at 0.67 Wb. The predicted inductance for the inductor is 0.40 H.

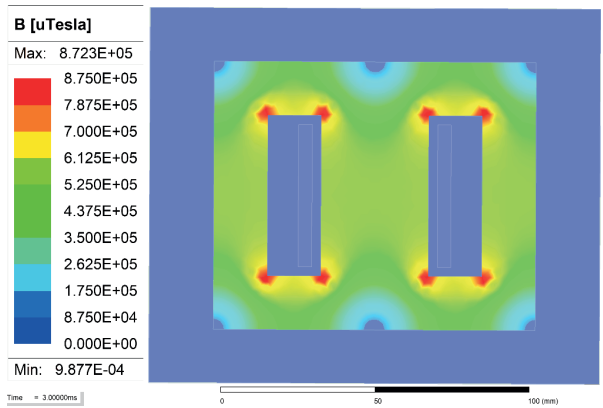

FIGURE 8. Density plot of magnetic flux density in the inductor: non-linear core with longitudinal parameters. The values of magnetic flux density are in microtesla.

6 | APPLICATION OF TRANSVERSAL PARAMETERS FOR AN INDUCTOR WITH A NON-LINEAR CORE

In this analysis, the procedures outlined in Section 4 were followed. The only variation occurred in the core, where a non-linear relative magnetic permeability was established, represented by an anisteretic *HB* curve in the ascending first quadrant H_yB_y.

Fig. 9 shows that the magnetic flux density is 0.00 T in the simulation region and coils, while in the eight corners of the core windows, the magnetic flux density reaches 0.91 T. In the core, the predominant magnetic flux density values range between 0.55 and 0.64 T. Another relevant result highlights the non-sinusoidal behavior of the flux linkage, current, and induced voltage over time. The maximum value of induced voltage is 125.91 V, the maximum current is 0.09 A, and the flux linkage peaks at 0.67 Wb. The estimated inductance for the inductor is 0.38 H.

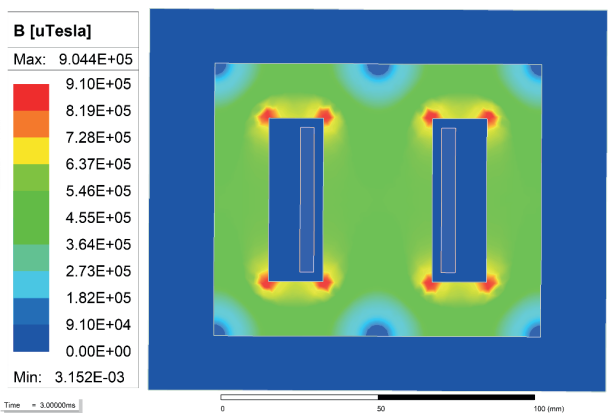

FIGURE 9. Density plot of magnetic flux density in the inductor: non-linear core with transverse parameters. The values of magnetic flux density are in microtesla.

The Jiles-Atherton model was used in this chapter because of its simplicity and widespread acceptance in the scientific community. However, its primary limitation is that it is better suited for *BH* curves that have a sigmoidal shape. For further information on the finite element method, it is advisable to refer to [20] and [25].

In the inductor simulations conducted using ANSYS software, an excitation voltage of 127 V was applied. In all instances, the voltages induced in the inductor were approximately 99.2% of this value. It is important to note that the under-voltage relay monitors the minimum permissible voltage and is configured to operate at 80% of the nominal voltage. The induced voltages remained above this 80% threshold.

7 | CONCLUSION

This chapter presented an improved methodology for identifying the ten parameters of the Jiles-Atherton hysteresis vector model. The genetic algorithms proved to be a fast and efficient approach, providing parameters that accurately describe the measured *HB* curves in both the longitudinal and transverse directions. An extensive comparison of the electrical and magnetic quantities of an alternating current inductor was also developed. The inductor was simulated with a non-linear anisotropic core and a non-linear isotropic core. In the case of the non-linear isotropic core, we considered the longitudinal and transverse directions separately. The obtained results show a significant change in the electric current value. In the anisotropic case, the current reaches a maximum of 0.07 A. In the longitudinal isotropic case, this value is 57.14% lower, and in the transverse isotropic case, it is 28.57% higher. The non-linear anisotropic analysis allowed for a more realistic simulation of the material's behavior and enabled the simultaneous analysis of different directions. This approach provides a more comprehensive and accurate understanding of the characteristics of the alternating current inductor. It's important to consider anisotropy for accurate modeling. Future works will address the saturation phenomenon, magnetic losses, and comparison with other methodologies.

DEDICATION

This work is dedicated to Maria de Fátima dos Ramos Rodrigues Mendes Barbosa.

ACKNOWLEDGMENT

We thank Ketty Keisy Barbosa Sobrado Suarez for her significant collaboration in accurately refining our figures.

I want to thank the Lord of Life, my family, friends, and colleagues, for their support, encouragement, and kindness throughout my journey.

REFERENCES

[1] D. C. Jiles e D. L. Atherton, “Theory of Ferromagnetic Hysteresis,” *Journal of Magnetism and Magnetic Materials,* vol. 61, pp. 48-60, 1986.

[2] D. C. Jiles, J. B. Thoelke e M. K. Devine, “Numerical Determination of Hysteresis Parameters the Modeling of Magnetic Properties Using the Theory of Ferromagnetic Hysteresis,” *IEEE Trans. Magn.,* vol. 28, pp. 27-35, Jan 1992.

[3] J. V. Leite, N. Sadowski, P. Kuo-Peng, N. J. Batistela e J. P. A. Bastos, “The Inverse Jiles–Atherton Model Parameters Identification,” *IEEE Trans. Magn.,* vol. 39, pp. 1397-1400, May 2003.

[4] P. Kis e A. Iványi, “Parameter Identification of Jiles–Atherton Model with Nonlinear Least-square Method,” *Physica B,* pp. 59-64, 2004.

[5] J. V. Leite, S. L. Avila, N. J. Batistela, W. P. Carpes Jr., N. Sadowski e J. P. A. Bastos, “Real Coded Genetic Algorithm for Jiles–Atherton Model Parameters Identification,” *IEEE Trans. Magn.,* vol. 40, pp. 888- 891, Mar 2004.

[6] K. Chwastek e J. Szczyglowski, “Identification of a Hysteresis Model Parameters with Genetic Algorithms,” *Mathematics and Computers in Simulation,* vol. 71, pp. 206-211, 2006.

[7] M. Toman, G. Stumberger e D. Dolinar, “Parameter Identification of the Jiles–Atherton Hysteresis Model Using Differential Evolution,” *IEEE Trans. Magn.,* vol. 44, pp. 1098-1101, Jun. 2008.

[8] R. Marion, R. Scorretti, N. Siauve, M. Raulet e L. Krähenbühl, “Identification of Jiles–Atherton Model Parameters Using Particle Swarm Optimization,” *IEEE Trans. Magn.,* vol. 44, pp. 894-897, Jun. 2008.

[9] K. Chwastek e J. Szczygowski, “An Alternative Method to Estimate the Parameters of Jiles–Atherton Model,” *Journal of Magnetism and Magnetic Materials,* vol. 314, pp. 47-51, 2007.

[10] N. Sadowski, N. J. Batistela, J. P. A. Bastos e M. Lajoie-Mazenc, “An Inverse Jiles-Atherton Model to Take Into Account Hysteresis in Time Stepping Finite Element Calculations,” *IEEE Trans. Magn.,* vol. 38, pp. 797-800, Mar. 2002.

[11] K. Hoffmann, J. P. A. Bastos, J. V. Leite, N. Sadowski e F. B. R. Mendes, “A Vector Jiles-Atherton Model for Improving the FEM Convergence,” *IEEE Transactions on Magnetics,* vol. 53, June 2017.

[12] A. Hrennikoff, “Solution of Problems of Elasticity by the Framework Method,” *J. Appl. Mech.,* pp. A169-A175, Dec. 1941.

[13] R. Courant, “Variational Methods for the Solution of Problems of Equilibrium and Vibration,” *Bull. Amer. Math. Soc.,* pp. 1-23, 1943.

[14] M. J. Turner, R. W. Clough, H. C. Martin e L. J. Topp, “Stiffness and Deflection Analysis of Complex Structures,” *Journal of the Aeronautical Sciences,* vol. 23, September 1956.

[15] O. C. Zienkiewicz e Y. K. Cheung, “Finite Element Solution of Field Problems,” *The Engineer,* pp. 507-510, September 1965.

[16] R. W. Clough, “Original Formulation of the Finite Element Method, Finite Elements in Analysis and Design,” *Elsevier,* vol. 7, pp. 89-101, 1990.

[17] H. Ochiai, K. Shigematsu, J. Imaoka e M. Yamamoto, “Finite Element Method Based Thermal Magnetic Core Characteristics Modeling and Thermal Simulation,” *Proceedings of ISIE,* pp. 320-324, 2022.

[18] K. Fonteyn, A. Belahcen, R. Kouhia, P. Rasilo e A. Arkkio, “FEM for Directly Coupled Magneto-mechanical Phenomena in Electrical Machines,” *IEEE Trans. Magn.,* vol. 46, pp. 2923-2926, 2010.

[19] B. Parreira, S. Rafael, A. Pires e P. C. Branco, “Obtaining the Magnetic Characteristics of an 8/6 Switched Reluctance Machine: from FEM Analysis to the Experimental Tests,” *IEEE Trans. Ind. Electron.,* vol. 52, pp. 1635-1643, 2005.

[20] J. P. A. Bastos e N. Sadowski, **Electromagnetic Modeling by Finite Element Methods**, Marcel Dekker, 2003.

[21] Z. Chen, Y. Yu e Y. Wang, “Parameter Identification of Jiles- Atherton Model Based on Levy Whale Optimization Algorithm,” *IEEE Access,* vol. 10, pp. 66711-66721, 2022.

[22] M. Zou, “Parameter Estimation of Extended Jiles-Atherton Hysteresis Model Based on ISFLA,” *IET Electric Power Applications,* vol. 14, pp. 212-219, 2020.

[23] K. Li, Z. Zhang, P. Wang, Y. Liu e J. Zeng, “A Novel 3D Simulation Prediction Model of Mechanical Properties of Ferromagnetic Materials via Incremental Permeability Method,” *Journal of Magnetism and Magnetic Materials,* vol. 536, 2021.

[24] B. B. Miranda, J. A. Malagoli e J. R. Camacho, “Optimization Techniques and Mathematical Modeling Applied to Reluctance Motors,” *Journal of Microwaves, Optoelectronics and Electromagnetic Applications,* vol. 21, pp. 368-391, 2022.

[25] Ansys® Electromagnetics Suite, Release 2022 R2, Help System, **Getting Started with Maxwell**: Transient Problem, Ansys, Inc.